Low-Density EEG Correction With Multivariate Decomposition and Subspace Reconstruction

(Article begins on next page)

29 April 2024

Low-Density EEG Correction With Multivariate Decomposition and Subspace Reconstruction

Pasquale Arpaia, *Senior Member, IEEE*, Antonio Esposito, *Member, IEEE*,
Angela Natalizio, *Member, IEEE*, Marco Parvis, *Fellow, IEEE*,
and Marisa Pesola

Abstract—A hybrid method is proposed for removing artifacts from electroencephalographic (EEG) signals. This relies on the integration of artifact subspace reconstruction (ASR) with multivariate empirical mode decomposition (EMD). The method can be applied when few EEG sensors are available, a condition in which existing techniques are not effective, and it was tested with two public datasets: 1) semisynthetic data and 2) experimental data with artifacts. One to four EEG sensors were taken into account, and the proposal was compared to both ASR and multivariate EMD (MEMD) alone. The proposed method efficiently removed muscular, ocular, or eye-blink artifacts on both semisynthetic and experimental data. Unexpectedly, the ASR alone also showed compatible performance on semisynthetic data. However, ASR did not work properly when experimental data were considered. Finally, MEMD was found less effective than both ASR and MEMD-ASR.

LOW-DENSITY CONTAMINATED EEG — MULTIVARIATE EMPIRICAL MODE DECOMPOSITION — IMFs GROUPING — LOW-DENSITY CLEANED EEG — ARTIFACT SUBSPACE RECONSTRUCTION

Index Terms— Artifact removal, electroencephalography, empirical mode decomposition (EMD), few sensors, low cost.
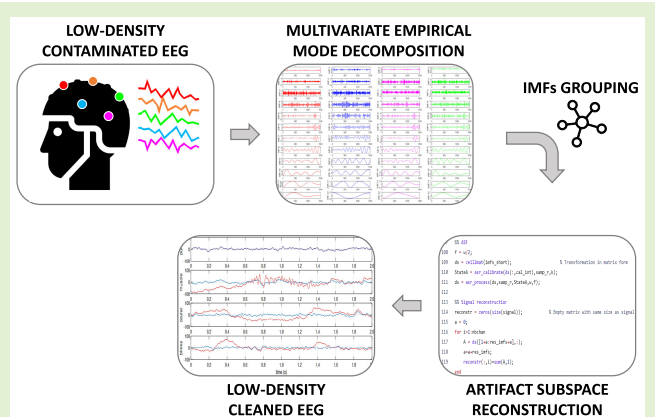
I. INTRODUCTION

ELECTROENCEPHALOGRAPHY (EEG) is a common and consolidated technique for measuring brain activity [1], [2]. The advantages of EEG are ease of use, non-invasiveness, wearability, and low cost [3], [4], [5]. Thanks to its flexibility, EEG has found application in clinical practice, research, and daily life, where a low number of sensors is desirable [6], [7], [8].

In out-of-the-lab contexts, however, artifacts of both endogenous and exogenous sources contaminate measured EEG signals [9], [10]. Among these, muscular and ocular artifacts are the most common and difficult to face. Artifact removal is essential to obtain a signal reflecting true brain activity, but the choice of a proper removal technique is not obvious, especially with few EEG sensors [11].

A suitable idea is to implement hybrid methods, that is, combining different rejection/removal techniques. This has been especially proposed for the few EEG sensor cases, in an attempt to merge the benefits of different techniques [12]. Several hybrid approaches involve a first step of data decomposition, to produce a higher-dimensional signal, and a subsequent artifact removal technique applicable to multidimensional signals.

Many approaches rely on empirical mode decomposition (EMD) [13], [14] and its modification [15]. Although these can be employed with simple component selection criteria [16], [17], the integration with techniques such as independent component analysis (ICA) [18] or canonical correlation analysis (CCA) [19] led to improved performance compared to single methods. However, they considered signals from multiple sensors decomposed individually.

In recent works, multivariate EMD (i.e., MEMD) was combined with CCA to remove only muscle artifacts from few sensors [20], [21]. It was demonstrated that this hybrid method outperforms multichannel CCA but with a higher

computational cost. Next, a faster version was proposed [22] by relying on fast MEMD [23]. The approach was only validated on actual EEG with a baseline contaminated by muscle artifacts, and further investigation should be carried on.

MEMD was also combined with ICA in removing only ocular artifacts from a five-sensor EEG [24]. An increase in the signal-to-noise ratio (SNR) was shown in both synthetic and experimental data. In [25], wavelet decomposition was applied after ICA on the components recognized as ocular artifacts, to preserve most of the actual EEG signal. This method was only tested on experimental data, and many sensing channels were needed for applying the ICA.

As a common limitation, the mentioned approaches specifically remove a single artifact type, that is, either muscular [19], [20], [21], [22], [26] or ocular [24], [27], [28], [29] ones. Nonetheless, the artifact removal technique should be applicable to a few-sensor scenario for different types of artifacts, since they can all occur during actual EEG acquisition. Despite its importance, such investigations are still scarce in the few-sensor scenario.

It should be noted that the above-mentioned methods combine modal decomposition with blind-source separation techniques. The latter relies on strict assumptions of independence of components to separate underlying sources [30], which is not always the case for modal decomposition. Instead, an adaptive filter such as the artifact subspace reconstruction (ASR) [31], [32], [33] has less strict assumptions and it already proved more effective in comparison with other methods [11].

Therefore, a novel hybrid method for artifact removal in low-density EEG setups is proposed. For the first time, the MEMD was combined with ASR to remove artifacts from a few available EEG signals and even in single-sensor settings. In particular, Section II provides a background on artifact removal, Section III introduces the proposed method, Section IV describes public data exploited for validating the method, and Section V discusses the results.

II. BACKGROUND

When dealing with EEG, artifact removal techniques can be classified into four main groups [12], [34]: regression-based, filtering, blind source separation, and source decomposition. In addition, new learning-based methods are recently receiving increasing attention [9], but these are beyond the present study.

Regression methods are still considered a gold standard, though they have been gradually replaced by more sophisticated methods. Meanwhile, *filtering methods* involve traditional frequency bandpass filters and adaptive ones. The former can be used if the bands of artifacts do not overlap with the signal of interest, while the latter are more flexible.

Simplicity and moderate computational costs are the main advantages of such techniques, while the need for a priori knowledge and/or reference channels are their major drawbacks. In this context, a recent and promising adaptive filtering technique is the ASR [31]: Extracts an artifact-free data fragment as a baseline and then corrects EEG data by setting an automatic threshold before reconstructing clean data. ASR computes a covariance matrix and retrieves statistics to identify and remove short, high-amplitude artifact components (e.g., muscle artifacts) [35].

Other artifact removal techniques can be classified as *blind source separation methods* and *source decomposition methods*. They do not require reference channels nor a priori knowledge about the artifacts, but they are based on strict assumptions of linearity, independence, and uncorrelation. In addition, they typically have high computational costs.

Blind source separation methods estimate a relationship matrix between the observed signals and the real unknown sources that generated them. The goal is to distinguish noise sources from real brain sources. Typical examples are the ICA, the CCA, or the principal component analysis (PCA). This category of techniques is often used in high-density biomedical signal processing [10], [30].

Source decomposition methods are based on the idea that the signal from each sensor can be decomposed into a series of fundamental modes in the time–frequency domain. Again, the noise components should be distinguishable in the transformed domain and removed before reconstructing the clean signal. Well-known examples are the wavelet transform [36] and the EMD [37]. In particular, EMD can only decompose 1-D signals independently. Meanwhile, the MEMD can decompose all the signals of a multidimensional acquisition at the same time by computing the same number of coherent modes for each sensor [38].

In a preliminary study [11], ICA, PCA, and ASR were compared while diminishing the number of available sensors. In accordance with the literature, ASR appeared as the most effective and balanced method when exploiting at least four sensors. Indeed, ASR was able to effectively correct the physiological artifacts while preserving a large part of the pure EEG signal and it was found to be the fastest technique (even ten times faster than ICA). However, its performance was degraded with less than four sensors. For the above reasons, Section III deals with the enhancement of ASR by means of MEMD.

III. PROPOSED METHOD

The proposed method aims to enable the usage of few EEG sensors. Similar to literature hybrid approaches, the few available signals are decomposed before applying a multidimensional artifact removal technique. However, using MEMD for that purpose is relatively new and the combination with ASR was unexplored.

A. Design

MEMD decomposition operates in a multivariate time–frequency domain and it gives back basic waveforms called intrinsic mode functions (IMFs) [38]. Different from EMD, the MEMD returns the same number of matched scale-aligned IMFs for each available signal. Artifacts could then be identified in the new space by applying ASR [31]. Notably, the ASR still relies on the statistics of a calibration interval, but retrieving statistics and cleaning must be done on IMFs.

To work properly, the MEMD and the ASR cannot be simply cascaded, but additional steps are necessary. Overall, the pipeline of the proposed hybrid method consists of five steps (Fig. 1):
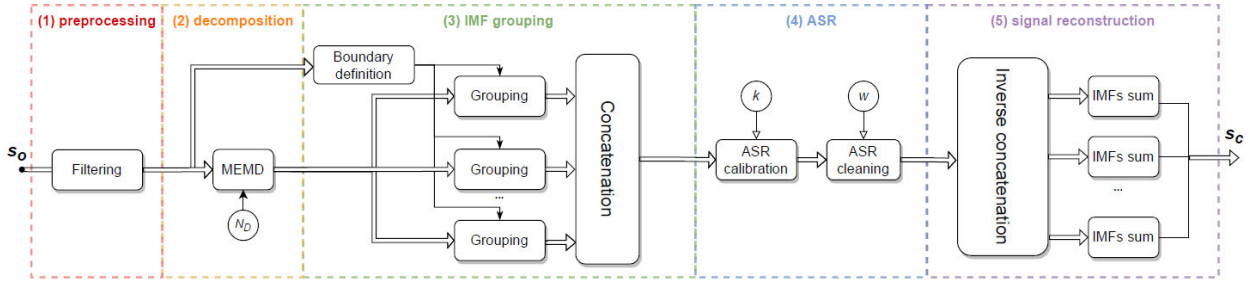
Fig. 1. Block diagram of the proposed hybrid method for artifact removal.

1) Preprocessing: The EEG signals are filtered in the frequency bands of interest and, after that, the epochs to analyze can be selected.

2) Decomposition: The MEMD is carried out on all the available EEG signals simultaneously. The number of directions of the signal projection should be explicitly fixed. To extract meaningful IMFs, this number must be greater than the dimensionality of the original signal. The rule adopted in the current proposal is

$$N_{\text{directions}} = 2 \times (N_{\text{sensors}} + 1) \qquad (1)$$

with the constraint of having at least six directions. This choice is consistent with the indications of the developers [39], [40]. At the end of the decomposition, the IMFs of each signal are matched among the corresponding sensors.

3) IMF Grouping: The resulting IMFs have many different amplitudes, which prevents the direct application of ASR. Therefore, IMFs with low amplitudes are identified and summed to the last IMF with acceptable amplitude. To set an amplitude boundary, a calibration interval before decomposition is taken into account and the difference Δ_p between the 90th and 10th percentile is calculated for each sensor. Then, the same quantity is calculated for all the IMFs associated with that calibration interval. If the interquartile range of an IMF is lower than 10% of Δ_p for at least one sensor, all the matched IMFs are summed up with the closest matched IMFs above the boundary. This process is done consistently for all sensors.

4) ASR: It includes a calibration phase and a cleaning phase. In this hybrid method, the calibration data are the IMFs obtained from the decomposition of the calibration interval. A mixing matrix M is obtained as the square root of the covariance matrix of calibration data. PCA is carried out for this mixing matrix. Then, a rejection threshold is automatically selected for each principal component as

$$\Gamma_i = \mu_i + k\sigma_i \qquad (2)$$

where μ_i and σ_i are the mean and standard deviation of the root mean square values obtained with a sliding window for each component. The threshold depends on the cut-off parameter k and the time window w on which statistics are calculated. For each window, the algorithm zeroes the components exceeding the rejection limit.

5) Signal Reconstruction: Once the data are cleaned with the ASR, the signals in the original space are reconstructed by the inverse MEMD, that is, the cleaned IMFs for each sensor are coherently summed up.

In the proposed method, calibration and artifacts data should be ideally recorded in compatible conditions, namely with the same acquisition hardware, in the same session, and with the same subject. However, calibration data from a previous session on the same subject could be reused.

Moreover, this hybrid method can also be applied to multidimensional signals with any number of sensors. Nonetheless, it should be noted that the number of IMFs passed to the ASR grows exponentially as the number of sensors increases.

B. Implementation

The proposed MEMD-ASR method was implemented as a MATLAB function, so that it can be easily integrated in EEG processing pipelines. The inputs of this function were as follows.

1) The *original signal* to be cleaned, expressed as an $(S \times N)$ matrix, where S is the number of samples and N is the number of sensors.
2) The *sampling frequency* of the original signal, expressed in samples per second.
3) The *calibration interval* corresponds to a time interval in which artifacts are assumed as absent.
4) The *cut-off parameter of ASR*, expressed as an integer greater than one; it determines the aggressiveness of data rejection: the smaller the k, the more the aggressiveness.
5) The *length of the statistics window*, expressed in seconds. This value w should be no longer than the time duration of the artifacts [31].

The output consists of the cleaned signal, still expressed as an $(S \times N)$ matrix.

Inside the function, the five steps described above were implemented. During signal preparation, a chunk of the signal had to be added at the end of the original signal. This typically consists of the last 0.25 s of the original signal that is flipped and concatenated. The reason is that the ASR cleaning function introduces a default delay due to a look-ahead operation. With this option, the ASR can reconstruct a sample by considering not only its preceding samples, but also the following ones [31]. Therefore, adding the chunk is needed whenever the look-ahead is exploited, while this will be removed in signal reconstruction by cutting the last 0.25 s.

The function implementing the MEMD was taken from [39], where the output IMFs are given as a cell per each sensor. These cells were converted into matrices, with rows corresponding to IMFs. Then, the grouping criterion was applied to reduce the number of IMFs to be passed to the ASR. Finally, the resulting IMFs per sensor were concatenated in a unique matrix.

TABLE I
CORRELATION COEFFICIENTS TO WEIGHT OCULAR ARTIFACTS AND EYE BLINKING FOR EACH SENSOR

Channel	Fp1	Fp2	F7	F3	Fz	F4	F8	C3	Cz	C4	P7	Pz	P8	O1	O2
Weight	0.87	1.00	0.59	0.25	0.73	0.44	0.47	0.24	0.00	0.12	0.35	0.26	0.27	0.31	0.28

Overall, reduced IMFs were obtained for either the calibration interval or the epochs with artifacts. These were given in input to the ASR, where the calibration function returns a state for initializing the subsequent cleaning phase. In addition to the state, the inputs for the cleaning phase are the data matrix, the sampling rate, the window length, and the look-ahead value. At the end of cleaning, the signal is reconstructed by summing the IMFs per sensor.

IV. DATASETS

The proposed method was validated on public semisynthetic and experimental datasets. Compared to purely synthetic data, semisynthetic data offer more realistic signal variability and power, ensuring reliability and results significance. To generate semisynthetic data, pure EEG data were first synthesized and then partially contaminated with artifacts extracted from real recordings. In doing so, the pure EEG can be easily compared with the cleaned EEG. This is indeed not possible with actual EEG data, but the results on them should be discussed differently.

A. Semisynthetic Data

Pure EEG signals were synthesized with the recently developed *SEED-G simulator* available online [41]. Per each sensor, a 150-s-long pure signal was generated with a sampling frequency of 256 Sa/s. These parameters were chosen to have suitable data for the application of the ASR. In detail, the first 60 s of the trace were left intact to represent clean calibration data. The remaining 90 s were contaminated with three types of artifacts: muscular, ocular, and eye blinking.

The muscular and ocular artifacts were extracted from the online *DenoiseNet database* [42]. These artifacts are available in 2-s-long segments at a sampling rate of 256 Sa/s, consistent with the choice made to simulate pure EEG. Therefore, 15 segments were randomly extracted for each artifact type to obtain 30 s of muscular artifacts and 30 s of ocular artifacts. In addition, eye blinking artifacts were added on the last 30 s of the signal. In this case, half sinusoidal signals with 0.2-s duration were added to simulate the typical eye blinking peaks. The time distance between them was set 1 s apart.

The amplitude of the synthetic artifacts was adjusted with respect to the pure synthetic signal to achieve an SNR from −20 to 5 dB [43]. Moreover, since ocular artifacts and eye blinking usually propagate over the scalp starting from the prefrontal area, their addition was weighted per channel. The weights were achieved as the correlation coefficients between real electrooculographic data and corresponding EEG data [41]. Fifteen channels were thus chosen from different regions of the scalp, and these are indicated in Table I with the mentioned correlation coefficients.

B. Experimental Data From a Public Dataset

A public dataset was exploited to extract actual EEG data [44]. This dataset is meant for testing artifact removal techniques and includes 13 participants with one recording session each. Brain signals were recorded by using a helmet by Brain Products [45] with 27 EEG channels and three electrooculographic channels, at a sampling rate of 200 Sa/s. Despite the nonwearability of the acquisition device, these publicly available data were chosen for the sake of reproducibility and the possibility of analyzing different numbers of sensors. The subjects sat in front of a screen to follow instructions for performing muscular or ocular artifacts.

Each experimental session consisted of two parts. First, the subjects were asked to focus on a fixation cross on the screen and avoid doing artifacts (baseline). Clean 30-s-long signals were thus recorded for each subject twice. Second, nine different artifact types were done in random order ten times each. A single trial with artifact lasted from 10 to 30 s, for a total length of 40–50 min for the second part.

In the present work, data from the first subject of the dataset were chosen to be processed. For computational reasons, the length of the entire EEG signal was limited to about 8 min. While the two sets of baseline signals were kept unchanged, only ten continuous artifact conditions were considered for the contaminated signal part. Finally, the whole EEG data were filtered in the 1–40-Hz range and base-normalized to have zero mean. Note that the last condition was also satisfied when generating semisynthetic data.

V. RESULTS AND DISCUSSION

The experimental setup is described in this section along with the metrics adopted for quantifying the method's effectiveness. The results presented hereafter can be reproduced by exploiting the code published at https://github.com/anthonyesp/low_density_eeg_asr.git.

A. Experimental Setup

In accordance with the above discussion, the proposed hybrid method was tested from four sensors down to a single sensor but can work properly with up to four sensors. Notably, in the case of a single sensor, the MEMD is actually an EMD. Per each number of sensors, the sensors were randomly selected 15× among available ones to obtain an average performance independent of their locations.

Different values for the cut-off parameter k and for the statistical window w associated with ASR were investigated to identify the best pair. Notably, k was varied from 5 to 30 with step 1 and w was varied from 0.2 to 3.0 s with step 0.1 s. The selection of the best ASR parameters was based on the relative root mean square error (RRMSE) [46]. It reflects the differences between the pure EEG signal and the EEG signal cleaned by MEMD-ASR. It is defined as

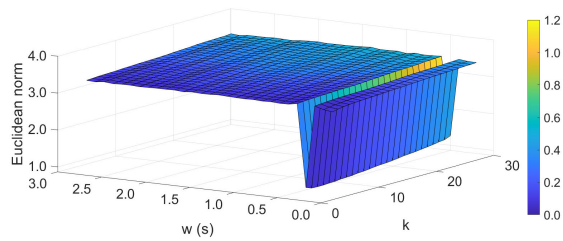$$\text{RRMSE} = \sqrt{\frac{\sum_{i=1}^{N}\left[\text{eeg}^{\star}(i) - \text{eeg}(i)\right]^2}{\sum_{i=1}^{N}\text{eeg}(i)^2}} \qquad (3)$$

Fig. 2. Surface obtained by calculating the Euclidean norm in 5-D space associated with the RRMSE in the two-sensor case.

TABLE II
MEDIAN RRMSE VALUES FOR SEMISYNTHETIC DATA

#sensors	method	w (s)	k	baseline	pure	muscle	ocular	blinks
4	MEMD	-	-	0.00	0.00	8.61	0.99	0.56
4	ASR	0.5	7	0.00	0.00	0.27	0.34	0.40
4	MEMD-ASR	0.5	9	0.00	0.00	0.60	0.30	0.46
3	MEMD	-	-	0.18	0.20	8.87	0.95	0.59
3	ASR	0.5	8	0.00	0.00	0.38	0.37	0.47
3	MEMD-ASR	0.5	8	0.01	0.00	0.70	0.34	0.45
2	MEMD	-	-	0.25	0.27	9.08	0.90	0.54
2	ASR	0.5	12	0.00	0.00	0.69	0.58	0.55
2	MEMD-ASR	0.5	9	0.00	0.00	0.70	**0.35**	0.45
1	EMD	-	-	0.27	0.31	9.24	0.65	0.62
1	EMD-ASR	0.5	12	0.00	0.00	1.25	0.50	0.59

bold: median RRMSE for MEMD-ASR significantly lower than respective ASR one.
w: length of the statistics window in seconds; k: cut-off parameter of ASR.

where eeg(i) and eeg$^\star(i)$ are samples of the uncontaminated signal and cleaned one, respectively. These values should be zero in the ideal case, that is, with artifacts perfectly removed.

Therefore, semisynthetic data were primarily used in these tests. RRMSE was calculated on different segments: the segment used as a baseline for ASR, the residual pure EEG (not used as a baseline), the segments with muscle artifacts, the one with ocular artifacts, and the one with blink artifacts.

The point defined by the five RRMSE values (as five were the EEG segments) was considered in a Euclidean 5-D space and its norm was calculated. The dispersion around these values was also taken into account and propagated to achieve the uncertainty of the norm. The optimal w was chosen to minimize the Euclidean norm and possibly its associated uncertainty. Then, k was identified by looking for the minimum 90th percentile associated with the five values. As an essential check, once w and k were fixed, a visual inspection of the signals in the time domain was carried on. In particular, the pure signal and the signal cleaned with MEMD-ASR were compared for each segment of the EEG signal.

Eventually, the hybrid method was tested on experimental data by using the best w and k chosen on semisynthetic data. Again, sensors were randomly selected $15\times$ from the available ones to test the method from four sensors down to a single sensor. To evaluate the effectiveness of the hybrid method on experimental data, a visual inspection of the signals in the time domain was carried out. The RRMSE was calculated too. Nonetheless, as the pure signal is not available with experimental data, this metric has the same meaning of the semisynthetic data case only when considering the baseline and pure segments. The same metric was calculated on the remaining segments with artifacts that are thus not reported to avoid misunderstandings.

B. Results on Semisynthetic Data

To identify the optimal k and w values, Fig. 2 shows the Euclidean 5-D norm associated with median RRMSE values. Moreover, its colors refer to the dispersion of the norm. This specific result regards the two-sensors case, but similar surfaces were obtained in the other cases.

As observed by the sharp negative peak, $w = 0.5$ s remained unaffected by both the k value and the number of sensors. This new w value corresponds to the default length of the statistics window [31], [47]. In addition, a value for k in the 5–10 range minimizes both the norm and its dispersion. After fixing w, the optimal value of k was identified as described in V-A

per each number of sensors. In general, for small k values, the baseline and pure segments differ from the original ones, but the artifacts are completely removed. On the other hand, for large k values, the baseline and pure segments match the original ones but the artifacts are only partially removed.

Table II reports the median RRMSE corresponding to the optimal w and k values. Moreover, the novel hybrid method was compared to ASR and MEMD alone. Note that the classical ASR cannot be applied to a single sensor as a method based on covariance [48], [49], thus EMD-ASR was only compared with EMD alone. Furthermore, entropy was used as a criterion to identify and remove artifactual IMFs, as proposed in [50]. These results demonstrate that the proposed hybrid method performs compatibly with the ASR. In contrast, the only MEMD is not effective in isolating artifacts but, due to its filter bank-like behavior [38], it affects clean signals.

The RRMSE values of Table II are also compatible with previous studies. Notably, by considering results on semisimulated data with an SNR between -20 and 5 dB, the RRMSE values reported in [20], [21], and [22] span in the 0.2–0.5 range. Moreover, it should be noted that the minimum number of considered channels was 3, even when taking into account other relevant studies [24], [40].

The Mann–Whitney U-test [51] was applied to prove differences between MEMD-ASR, ASR, and MEMD with a 5% significance level. The test results confirmed that the medians of RRMSE for ASR are not significantly different from MEMD-ASR, except for the case of an ocular artifact with two sensors (reported in bold). Meanwhile, they also confirmed that MEMD performs worse than both MEMD-ASR and ASR.

The gain in the signal-to-artifact ratio (γ) [46] was then investigated as a further metric. Notably, this could be only exploited on semisynthetic data as it requires the availability of the true EEG. The γ is defined as

$$\gamma = 10 \log \frac{\sum_{n=1}^{N} \left| \text{eeg}^\diamond(i) - \text{eeg}(i) \right|^2}{\sum_{n=1}^{N} \left| \text{eeg}^\star(i) - \text{eeg}(i) \right|^2} \quad (4)$$

where eeg$^\diamond(i)$ are the samples of the contaminated EEG signal. Positive values of gamma indicate a better SNR, negative values indicate a decrease, and zero represents no improvement. Table III reports the median γ, corresponding to the optimal w and k values, in comparing the novel hybrid method with ASR and MEMD alone.

Since the contaminated signal eeg$^\diamond(i)$ and the uncontaminated signal eeg(i) coincide within the baseline and pure

TABLE III
MEDIAN γ VALUES FOR SEMISYNTHETIC DATA

#sensors	method	w (s)	k	muscle	ocular	blinks
4	MEMD	-	-	0.00	0.00	0.00
4	ASR	0.5	7	29.70	12.66	6.33
4	MEMD-ASR	0.5	9	23.85	13.63	5.37
3	MEMD	-	-	0.50	1.64	0.76
3	ASR	0.5	8	27.12	12.41	4.84
3	MEMD-ASR	0.5	8	22.64	12.88	5.40
2	MEMD	-	-	0.95	0.63	0.54
2	ASR	0.5	12	22.47	5.37	0.00
2	MEMD-ASR	0.5	9	21.01	**9.58**	**1.85**
1	EMD	-	-	1.07	5.03	2.19
1	EMD-ASR	0.5	12	16.31	6.50	0.00

bold: median γ for MEMD-ASR significantly higher than respective ASR one.
w: length of the statistics window in seconds; k: cut-off parameter of ASR.

TABLE IV
MEDIAN RRMSE FOR EXPERIMENTAL DATA

#sensors	method	w (s)	k	baseline	pure
4	MEMD	-	-	0.94	0.94
4	ASR	0.5	7	0.90	0.90
4	MEMD-ASR	0.5	9	**0.32**	**0.28**
3	MEMD	-	-	1.01	1.01
3	ASR	0.5	8	1.14	1.14
3	MEMD-ASR	0.5	8	**0.34**	**0.40**
2	MEMD	-	-	0.80	0.75
2	ASR	0.5	12	0.94	0.98
2	MEMD-ASR	0.5	9	**0.19**	**0.28**
1	EMD	-	-	0.72	0.67
1	EMD-ASR	0.5	12	0.18	0.15

bold: median RRMSE for MEMD-ASR significantly lower than respective ASR.
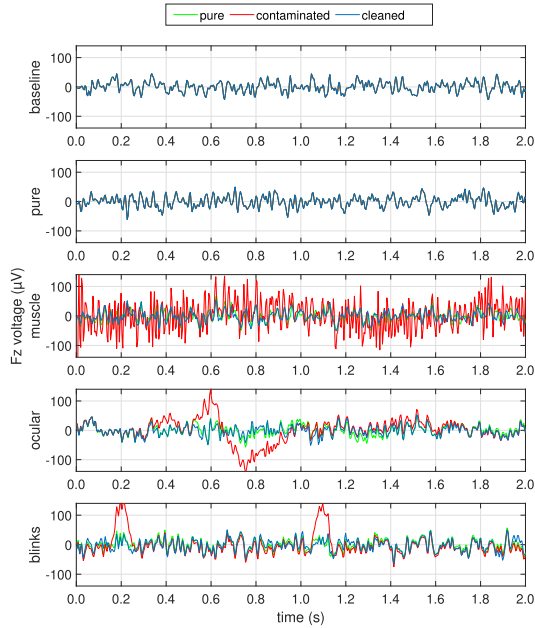w: length of the statistics window in seconds; k: cut-off parameter of ASR.

Fig. 3. Visual inspection of the sensor Fz with two sensors involved in artifact removal by MEMD-ASR. Quantitative metrics associated with these semisynthetic data are reported in Tables II and III.
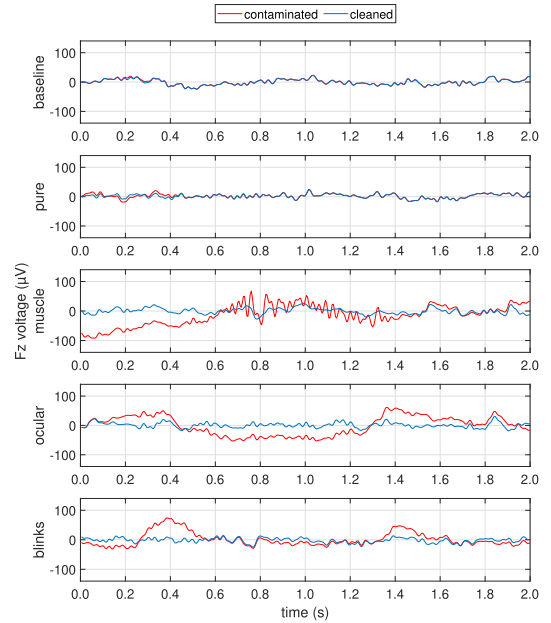

Fig. 4. Visual inspection of the sensor Fz with two sensors involved in artifact removal by MEMD-ASR. Quantitative metrics associated with these experimental data are reported in Table IV.

segments, γ was computed only for the three artifact conditions. Also in this case, statistical testing proved the superior performance of MEMD-ASR over ASR for eye blinks, but also for ocular artifacts, in the two sensors case. In all other cases, MEMD-ASR and ASR demonstrated compatible performance and both were better than only MEMD.

Visual inspection confirmed that MEMD-ASR and ASR have compatible performance on these data. Meanwhile, EMD-ASR is effective in removing ocular and eye-blink artifacts on single-channel EEG. Fig. 3 shows a representative example of visual inspection. The two-sensor case was considered and the sensor Fz is here represented with respect to the five EEG segments. As expected, the green (pure signal) and the blue (signal cleaned with MEMD-ASR) curves are mostly overlapped. Hence, artifacts are removed with respect to the red curves representing contaminated signals.

C. Results on Experimental Data From the Public Dataset

As anticipated, the optimal w and k values derived with the semisynthetic data were adopted on experimental data too.

Table IV reports, for the only baseline and pure data segments, the median RRMSE corresponding to the same w and k values of Table II. The novel method was again compared to MEMD and ASR. The proposed hybrid method affects the baseline and the pure signal segment less than both MEMD and ASR alone, with a significant difference for all cases from four to two sensors.

An example of the effectiveness of MEMD-ASR in removing artifacts is reported in Fig. 4. The two-sensor case was considered and the sensor Fz is here represented with respect to the five EEG segments. The signals cleaned with MEMD-ASR (blue) are here compared to the experimental data signals (red). It can be seen that these signals are mostly overlapped in the baseline and pure conditions, while artifacts are removed in the other three conditions. The effectiveness of the proposed methods is further supported by the visual inspection of baseline and ocular artifacts for comparing the artifact removal methods (Fig. 5). In there, the two-sensor case was again involved. In the calibration segment neither MEMD nor MEMD-ASR affects the signal, while the ASR already disrupts it. Regarding the noisy segment, the MEMD-ASR is
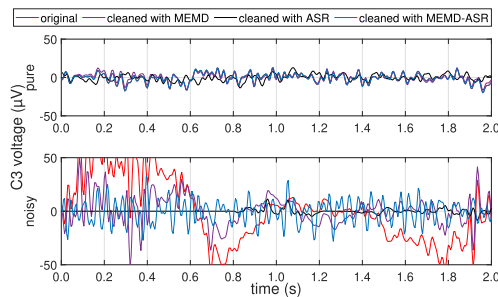
Fig. 5. Visual inspection of the sensor C3 with two sensors involved in comparing artifact removal methods. Quantitative metrics associated with these experimental data are reported in Table IV.

the only one to effectively remove ocular artifacts. Conversely, the MEMD fails to mitigate artifacts and the ASR overcorrects them. Indeed, the ASR fails to remove artifacts and cancels out the signal on experimental data, in contrast to its performance on semisynthetic data.

In conclusion, it should be noted that a drawback of the proposed technique is execution time. ASR alone takes about 0.2–0.4 s to remove artifacts, where the more the sensor the higher the time. Meanwhile, MEMD-ASR execution takes from about 32 s (two sensors) to about 72 s (four sensors). Instead, EMD-ASR for a single sensor takes about 0.7 s. The MEMD thus creates a bottleneck in terms of processing time, but the EMD-ASR discloses the possibility of implementing a soft EEG sensor with integrated artifact removal features.

D. From Semisynthetic to Experimental Data

Results on semisynthetic data suggest that ASR is equally or more effective than MEMD-ASR down to two sensors. Meanwhile, a significant improvement with MEMD-ASR holds for the removal of ocular artifacts in the two-sensor case. This was confirmed with statistical testing on both RRMSE and γ metrics. In contrast, MEMD alone was always found to be less effective than ASR and MEMD-ASR. Compared with ASR alone, the proposed method discloses the possibility of working on a single sensor. However, EMD-ASR does not seem effective in removing blinks.

Conversely, when experimental data were used, the MEMD-ASR appeared more effective than ASR and MEMD in not affecting the baseline and pure EEG signal. Furthermore, the visual inspection in Fig. 4 proves that the hybrid approach exhibits a balanced corrective action. Meanwhile, in accordance with literature [38], MEMD fails to remove artifacts in the same frequency bands of the signal.

Finally, Fig. 5 supports the importance of testing artifact removal techniques on experimental data despite the unknown pure EEG. Notably, the only RRMSE would not highlight the issue, thus confirming the importance of visual inspection in the current scenario.

VI. CONCLUSION

This work has proposed a hybrid artifact removal method addressed to low-density EEG. Different from existing literature, this was designed to remove various types of EEG artifacts and to jointly consider all the available channels for maximizing the available information. The method relies on the multivariate version of EMD and ASR.

Both semisynthetic and experimental data were exploited to validate the method. In the former case, the hybrid method has performance compatible with the classical ASR. In the latter case, visual inspection demonstrated that ASR is not effective on experimental data, while only MEMD-ASR works properly. This also suggested that semisynthetic data are not always appropriate for testing artifact removal techniques. Finally, MEMD was found to be less effective than MEMD-ASR and ASR.

Future works should further explore the applicability of the proposed methods in different settings. Moreover, execution time should also be reduced if willing to realize soft sensors for online applications. Finally, standardization in terms of metrics is still required, especially when experimental data are used. These speculations will be eased by the material shared for the present article to replicate and extend the results.

REFERENCES

[1] M. Teplan, "Fundamentals of EEG measurement," *Meas. Sci. Technol.*, vol. 2, no. 2, pp. 1–11, 2002.

[2] J. S. Kumar and P. Bhuvaneswari, "Analysis of electroencephalography (EEG) signals and its categorization—A study," *Proc. Eng.*, vol. 38, pp. 2525–2536, 2012.

[3] P. Arpaia, E. De Benedetto, C. A. Dodaro, L. Duraccio, and G. Servillo, "Metrology-based design of a wearable augmented reality system for monitoring patient's vitals in real time," *IEEE Sensors J.*, vol. 21, no. 9, pp. 11176–11183, May 2021.

[4] P. Arpaia, E. De Benedetto, L. De Paolis, G. D'Errico, N. Donato, and L. Duraccio, "Performance enhancement of wearable instrumentation for AR-based SSVEP BCI," *Measurement*, vol. 196, Jun. 2022, Art. no. 111188.

[5] A. Apicella et al., "Enhancement of SSVEPs classification in BCI-based wearable instrumentation through machine learning techniques," *IEEE Sensors J.*, vol. 22, no. 9, pp. 9087–9094, May 2022.

[6] A. E. Hramov, V. A. Maksimenko, and A. N. Pisarchik, "Physical principles of brain–computer interfaces and their applications for rehabilitation, robotics and control of human brain states," *Phys. Rep.*, vol. 918, pp. 1–133, Jun. 2021.

[7] P. Arpaia, L. Callegaro, A. Cultrera, A. Esposito, and M. Ortolano, "Metrological characterization of consumer-grade equipment for wearable brain computer interfaces and extended reality," *IEEE Trans. Instrum. Meas.*, vol. 71, pp. 1–9, 2022.

[8] P. Sawangjai, S. Hompoonsup, P. Leelaarporn, S. Kongwudhikunakorn, and T. Wilaiprasitporn, "Consumer grade EEG measuring sensors as research tools: A review," *IEEE Sensors J.*, vol. 20, no. 8, pp. 3996–4024, Apr. 2020.

[9] J. Minguillon, M. A. Lopez-Gordo, and F. Pelayo, "Trends in EEG-BCI for daily-life: Requirements for artifact removal," *Biomed. Signal Process. Control*, vol. 31, pp. 407–418, Jan. 2017.

[10] W. Mumtaz, S. Rasheed, and A. Irfan, "Review of challenges associated with the EEG artifact removal methods," *Biomed. Signal Process. Control*, vol. 68, Jul. 2021, Art. no. 102741.

[11] P. Arpaia, E. De Bendetto, A. Esposito, A. Natalizio, M. Parvis, and M. Pesola, "Comparing artifact removal techniques for daily-life electroencephalography with few channels," in *Proc. IEEE Int. Symp. Med. Meas. Appl. (MeMeA)*, Jun. 2022, pp. 1–6.

[12] J. A. Urigüen and B. Garcia-Zapirain, "EEG artifact removal-state-of-the-art and guidelines," *J. neural Eng.*, vol. 12, no. 3, 2015, Art. no. 031001. .

[13] A.-O. Boudraa and J.-C. Cexus, "EMD-based signal filtering," *IEEE Trans. Instrum. Meas.*, vol. 56, no. 6, pp. 2196–2202, Dec. 2007.

[14] A. Komaty, A.-O. Boudraa, B. Augier, and D. Daré-Emzivat, "EMD-based filtering using similarity measure between probability density functions of IMFs," *IEEE Trans. Instrum. Meas.*, vol. 63, no. 1, pp. 27–34, Jan. 2014.

[15] Z. Wu and N. E. Huang, "Ensemble empirical mode decomposition: A noise-assisted data analysis method," *Adv. Adapt. Data Anal.*, vol. 1, no. 1, pp. 1–41, Jan. 2009.

[16] P. Gaur, R. B. Pachori, H. Wang, and G. Prasad, "An automatic subject specific intrinsic mode function selection for enhancing two-class EEG-based motor imagery-brain computer interface," *IEEE Sensors J.*, vol. 19, no. 16, pp. 6938–6947, Aug. 2019.

[17] O. A. Omitaomu, V. A. Protopopescu, and A. R. Ganguly, "Empirical mode decomposition technique with conditional mutual information for denoising operational sensor data," *IEEE Sensors J.*, vol. 11, no. 10, pp. 2565–2575, Oct. 2011.

[18] K. Zeng, D. Chen, G. Ouyang, L. Wang, X. Liu, and X. Li, "An EEMD-ICA approach to enhancing artifact rejection for noisy multivariate neural data," *IEEE Trans. Neural Syst. Rehabil. Eng.*, vol. 24, no. 6, pp. 630–638, Jun. 2016.

[19] X. Chen, A. Liu, J. Chiang, Z. J. Wang, M. J. McKeown, and R. K. Ward, "Removing muscle artifacts from EEG data: Multichannel or single-channel techniques?" *IEEE Sensors J.*, vol. 16, no. 7, pp. 1986–1997, Apr. 2016.

[20] X. Xu, A. Liu, and X. Chen, "A novel few-channel strategy for removing muscle artifacts from multichannel EEG data," in *Proc. IEEE Global Conf. Signal Inf. Process. (GlobalSIP)*, Nov. 2017, pp. 976–980.

[21] X. Chen, X. Xu, A. Liu, M. J. McKeown, and Z. J. Wang, "The use of multivariate EMD and CCA for denoising muscle artifacts from few-channel EEG recordings," *IEEE Trans. Instrum. Meas.*, vol. 67, no. 2, pp. 359–370, Feb. 2018.

[22] Y. Liu et al., "An efficient and robust muscle artifact removal method for few-channel EEG," *IEEE Access*, vol. 7, pp. 176036–176050, 2019.

[23] X. Lang et al., "Fast multivariate empirical mode decomposition," *IEEE Access*, vol. 6, pp. 65521–65538, 2018.

[24] G. Wang, C. Teng, K. Li, Z. Zhang, and X. Yan, "The removal of EOG artifacts from EEG signals using independent component analysis and multivariate empirical mode decomposition," *IEEE J. Biomed. Health Informat.*, vol. 20, no. 5, pp. 1301–1308, Sep. 2016.

[25] N. Al-Qazzaz, S. H. B. M. Ali, S. Ahmad, M. Islam, and J. Escudero, "Automatic artifact removal in EEG of normal and demented individuals using ICA–WT during working memory tasks," *Sensors*, vol. 17, no. 6, p. 1326, Jun. 2017.

[26] X. Chen, Q. Chen, Y. Zhang, and Z. J. Wang, "A novel EEMD-CCA approach to removing muscle artifacts for pervasive EEG," *IEEE Sensors J.*, vol. 19, no. 19, pp. 8420–8431, Oct. 2019.

[27] R. Ranjan, B. C. Sahana, and A. K. Bhandari, "Ocular artifact elimination from electroencephalography signals: A systematic review," *Biocybernetics Biomed. Eng.*, vol. 41, no. 3, pp. 960–996, Jul. 2021.

[28] A. K. Maddirala and R. A. Shaik, "Removal of EOG artifacts from single channel EEG signals using combined singular spectrum analysis and adaptive noise canceler," *IEEE Sensors J.*, vol. 16, no. 23, pp. 8279–8287, Dec. 2016.

[29] R. Patel, M. P. Janawadkar, S. Sengottuvel, K. Gireesan, and T. S. Radhakrishnan, "Suppression of eye-blink associated artifact using single channel EEG data by combining cross-correlation with empirical mode decomposition," *IEEE Sensors J.*, vol. 16, no. 18, pp. 6947–6954, Sep. 2016.

[30] C. Stergiadis, V.-D. Kostaridou, and M. A. Klados, "Which BSS method separates better the EEG signals? A comparison of five different algorithms," *Biomed. Signal Process. Control*, vol. 72, Feb. 2022, Art. no. 103292.

[31] T. R. Mullen et al., "Real-time neuroimaging and cognitive monitoring using wearable dry EEG," *IEEE Trans. Biomed. Eng.*, vol. 62, no. 11, pp. 2553–2567, Nov. 2015.

[32] S. Blum, N. S. J. Jacobsen, M. G. Bleichner, and S. Debener, "A Riemannian modification of artifact subspace reconstruction for EEG artifact handling," *Frontiers Human Neurosci.*, vol. 13, p. 141, Apr. 2019.

[33] A. Cataldo et al., "A method for optimizing the artifact subspace reconstruction performance in low-density EEG," *IEEE Sensors J.*, vol. 22, no. 21, pp. 21257–21265, Nov. 2022.

[34] K. Zeng and X. Li, "Artifact removal in EEG recordings," in *Signal Process. Neurosciences*. Cham, Switzerland: Springer, 2016, pp. 77–98.

[35] X. Chen et al., "Removal of muscle artifacts from the EEG: A review and recommendations," *IEEE Sensors J.*, vol. 19, no. 14, pp. 5353–5368, Jul. 2019.

[36] M. Unser and A. Aldroubi, "A review of wavelets in biomedical applications," *Proc. IEEE*, vol. 84, no. 4, pp. 626–638, Apr. 1996.

[37] N. E. Huang et al., "The empirical mode decomposition and the Hilbert spectrum for nonlinear and non-stationary time series analysis," *Proc. Roy. Soc. London. A, Math., Phys. Eng. Sci.*, vol. 454, no. 1971, pp. 903–995, Mar. 1998.

[38] D. P. Mandic, N. U. Rehman, Z. Wu, and N. E. Huang, "Empirical mode decomposition-based time-frequency analysis of multivariate signals: The power of adaptive data analysis," *IEEE Signal Process. Mag.*, vol. 30, no. 6, pp. 74–86, Nov. 2013.

[39] Y. Zhang et al., "Noise-assisted multivariate empirical mode decomposition for multichannel EMG signals," *Biomed. Eng. OnLine*, vol. 16, no. 1, pp. 1–17, Dec. 2017.

[40] Y. Zhang et al., "Noise-assisted multivariate empirical mode decomposition for multichannel EMG signals," *Biomed. Eng. OnLine*, vol. 16, no. 1, pp. 1–17, Dec. 2017.

[41] A. Anzolin, J. Toppi, M. Petti, F. Cincotti, and L. Astolfi, "SEED-G: Simulated EEG data generator for testing connectivity algorithms," *Sensors*, vol. 21, no. 11, p. 3632, May 2021.

[42] *EEGdenoiseNet*. Accessed: Sep. 2022. [Online]. Available: https://github.com/ncclabsustech/EEGdenoiseNet

[43] M. Dora and D. Holcman, "Adaptive single-channel EEG artifact removal with applications to clinical monitoring," *IEEE Trans. Neural Syst. Rehabil. Eng.*, vol. 30, pp. 286–295, 2022.

[44] S. Ehrlich. *Dataset—Automatic Artifact Removal*. Accessed: Sep. 2022. [Online]. Available: https://github.com/stefan-ehrlich/dataset-automaticArtifactRemoval

[45] *Introducing the Actichamp Plus–Offering Active and Passive Electrode Recordings and More!*. Accessed: Sep. 2022. [Online]. Available: https://pressrelease.brainproducts.com/actichamp_plus/

[46] M. M. N. Mannan, M. A. Kamran, and M. Y. Jeong, "Identification and removal of physiological artifacts from electroencephalogram signals: A review," *IEEE Access*, vol. 6, pp. 30630–30652, 2018.

[47] *Clean_Rawdata EEGLAB Plug-In*. Accessed: Sep. 2022. [Online]. Available: https://github.com/sccn/clean_rawdata

[48] C.-Y. Chang, S.-H. Hsu, L. Pion-Tonachini, and T.-P. Jung, "Evaluation of artifact subspace reconstruction for automatic artifact components removal in multi-channel EEG recordings," *IEEE Trans. Biomed. Eng.*, vol. 67, no. 4, pp. 1114–1121, Apr. 2020.

[49] V. P. Kumaravel, V. Kartsch, S. Benatti, G. Vallortigara, E. Farella, and M. Buiatti, "Efficient artifact removal from low-density wearable EEG using artifacts subspace reconstruction," in *Proc. 43rd Annu. Int. Conf. IEEE Eng. Med. Biol. Soc. (EMBC)*, Nov. 2021, pp. 333–336.

[50] Q. Liu, Y.-F. Chen, S.-Z. Fan, M. F. Abbod, and J.-S. Shieh, "EEG artifacts reduction by multivariate empirical mode decomposition and multiscale entropy for monitoring depth of anaesthesia during surgery," *Med. Biol. Eng. Comput.*, vol. 55, no. 8, pp. 1435–1450, Aug. 2017.

[51] P. E. McKnight and J. Najab, "Mann-whitney u test," in *The Corsini Encyclopedia of Psychology*. Cham, Switzerland: Springer, 2010, p. 923.

Pasquale Arpaia (Senior Member, IEEE) received the M.S. and Ph.D. degrees in electrical engineering from the University of Napoli Federico II, Naples, Italy, in 1988 and 1992, respectively.

He is a Full Professor of Instrumentation and Measurements with the University of Napoli Federico II.

Antonio Esposito (Member, IEEE) received the M.S. degree in electronic engineering from the University of Naples Federico II, Naples, Italy, in 2017, and the Ph.D. degree in metrology from Politecnico di Torino, Turin, Italy, in 2022.

His research activities focus on the wearable brain–computer interfaces.

Angela Natalizio (Member, IEEE) received the M.S. degree in biomedical engineering from the University of Naples Federico II, Naples, Italy, in 2019. She is pursuing the Ph.D. degree in metrology with the Politecnico di Torino, Turin, Italy.

Her research activities focus on the motor imagery-based brain–computer interfaces.

Marco Parvis (Fellow, IEEE) received the M.S. degree in electrical engineering and the Ph.D. degree in metrology from Politecnico di Torino, Turin, Italy, in 1982 and 1987, respectively.

He is a Full Professor of Electronic Measurements with the Politecnico di Torino.

Marisa Pesola received the M.S. degree in biomedical engineering from the University of Napoli Federico II, Naples, Italy, in 2022, where she is currently pursuing the Ph.D. degree in computational and quantitative biology.

Her research interests focus on the processing of biomedical signals and artifact removal.